An efficient multi-objective optimization strategy for Halbach array permanent magnet synchronous machines based on nonlinear semi-analytical model

Du, Yunlu; Huang, Yunkai; Guo, Baocheng; Zhu, Zichong; Peng, Fei; Dong, Jianning

DOI
10.3233/JAE-230029

Publication date
2023

Document Version
Final published version

Published in
International Journal of Applied Electromagnetics and Mechanics

International Journal of Applied Electromagnetics and Mechanics 73 (2023) 111–128
DOI 10.3233/JAE-230029
IOS Press

An efficient multi-objective optimization strategy for Halbach array permanent magnet synchronous machines based on nonlinear semi-analytical model

Yunlu Du[a], Yunkai Huang[a,*], Baocheng Guo[b], Zichong Zhu[c], Fei Peng[a] and Jianning Dong[d]
[a]*School of Electrical Engineering, Southeast University, Nanjing, China*
[b]*School of Electrical and Automation Engineering, Nanjing Normal University, Nanjing, China*
[c]*School of Electrical Engineering and Control Science, Nanjing Tech University, Nanjing, China*
[d]*Faculty of Electrical Engineering, Delft University of Technology, Delft, Netherlands*

Abstract. In this article, an efficient multi-objective optimization strategy for the Halbach array permanent magnet synchronous machine (PMSM) is developed by taking into consideration the nonlinear B-H behavior of soft magnetic materials. Based on the harmonic modeling (HM) technology, the electromagnetic performances (EPs) of the Halbach array PMSM can be computed. To specifically model the local magnetic saturation, the stator teeth are separated into several annular layers, and each tooth is further divided into several regions along the tangential direction. Then, the parameters of the Halbach array PMSM are optimized utilizing combined nonlinear semi-analytical model (SAM) and non-dominated sorting genetic algorithm II (NSGA-II). To validate the effectiveness and accuracy of the developed optimization scheme, a Halbach array prototype is then manufactured in accordance with the optimization results. The multi-objective rapid optimization strategy developed in this article, which includes but is not limited to Halbach array permanent magnet (PM) machines, serves as a reference for the design and optimization of various PM machines.

Keywords: Halbach array, permanent magnet synchronous machine (PMSM), magnetic saturation, non-dominated sorting genetic algorithm II (NSGA-II)

1. Introduction

Due to their excellent dynamic performances, permanent magnet (PM) machines are commonly utilized in industrial equipment and household appliances, such as submarine drives [1], electric vehicles [2–4], and flywheel energy storage systems [5]. The Halbach magnet array, which has good self-shielding magnetization characteristics, is frequently utilized in PM machines to decrease the harmonic content of air gap flux density and enhance torque density [6]. Despite the fact that the finite element (FE) analysis is an useful technique for accurately predicting the magnetic field for PM machines by taking into consideration the nonlinearity of materials and complex geometries, it is too time-consuming and inefficient for Halbach array PM machine optimization [7]. The alternative technique is the analytical method with a fast magnetic field prediction capacity [8].

*Corresponding author: Yunkai Huang, School of Electrical Engineering, Southeast University, Nanjing, 210096, China. E-mail: huangyk@seu.edu.cn.

On the other hand, even though the computation speed of the traditional exact sub-domain model (SDM) is fast, the effect of the nonlinearity of ferromagnetic materials cannot be considered; that is, the traditional SDM assumes that the relative permeability of the iron core is infinite [9]. To solve the aforementioned issue, [10,11] develop a nonlinear semi-analytical model (SAM). This scientific contribution has been utilized in the magnetic field prediction and electromagnetic performances (EPs) computation of switched reluctance machines [12,13], flux-modulated PM synchronous machines [14], axial flux machines [15,16], etc. Previous studies have demonstrated that the nonlinear SAM will be an effective technique for the fast evaluation of magnetic field distribution (MFD) and EPs of the Halbach array PMSMs.

Additionally, the majority of electric machine designs involve multi-objective optimization to minimize or maximize performance functions simultaneously [17]. Researchers have developed diverse optimization algorithms, such as Taguchi–chicken swarm optimization (Taguchi–CSO), fusion algorithm [18], genetic algorithm (GA) [19], particle swarm optimization (PSO) [20], and non-dominated sorting genetic algorithm II (NSGA-II) [21], to solve complex electric machine optimization problems. Based on the canonical PSO method, [22] proposes an optimization algorithm considering the nonlinearity of ferromagnetic materials of surface-mounted PM machines. Ref [23] proposes an online data-driven multi-objective optimization method, which adopts a two-loop optimization process, and the optimized results achieve 64% thrust ripple reduction and 6.6% average thrust increase, respectively. To maximize production quality and minimize the manufacturing cost of PM machines, a multilevel robust optimization method is proposed in [24]. To reduce the usage of rare-earth PMs, [25] proposes a multi-objective stratified optimization strategy. In these studies, the optimal design of electric machines is primarily based on the FE model, and the optimization requires a large number of iterations, which is quite time-consuming and complicated. Furthermore, there is still a scarcity of research on the fast optimization strategy of PM motors combined with analytical approach and optimization algorithm, especially for Halbach magnet array. As a result, a rapid optimization analytical framework of the electric machine is necessary, particularly for the Halbach array PM machine, whose structural parameters and magnetization direction need to be optimized.

To fill this gap, an efficient multi-objective optimization strategy for the Halbach array PM machine is developed in this article, which is based on the combined HM technology and NSGA-II optimization algorithm. In particular, the developed nonlinear SAM can consider the nonlinearity of ferromagnetic materials by an iterative algorithm. The FE models and experiments verify the effectiveness of the optimization cases.

This paper is organized as follows. Section 2 introduces the geometric structure of the studied Halbach array PMSM. The detailed description of the nonlinear SAM of the Halbach array PMSM is presented in Sections 3. The effective multi-objective optimization strategy that combines nonlinear SAM and NSGA-II is developed in Section 4. Then, Section 5 verifies the correctness of the optimization results by the FE analysis and experiments. Section 6 concludes this paper.

2. Studied machine

The basic geometry parameters of the studied Halbach array PM machine in this article are shown in Table 1. The stator slot is simplified in the analytical model to have an equal angle width. Therefore, the 2-D analytical model of the Halbach array PM machine, as illustrated in Fig. 1, can be obtained. In this article, each pole of the studied Halbach array PMSM is consisting of three PMs with different magnetization directions to decrease the harmonics of the air gap magnetic field and the eddy current loss

Table 1
Basic parameters of the studied Halbach array PM motor

Items	Symbol	Value
Number of stator slots	Q_s	12
Number of pole pairs	p	5
Radius of slot bottom	R_{sb}	74 mm
Radius of slot top	R_{st}	53.5 mm
Radius of stator bore	R_s	52 mm
Slot width angle	θ_{ss}	20°
Number of turns	N_c	16
Remanence of PM	B_{rem}	0.75 T

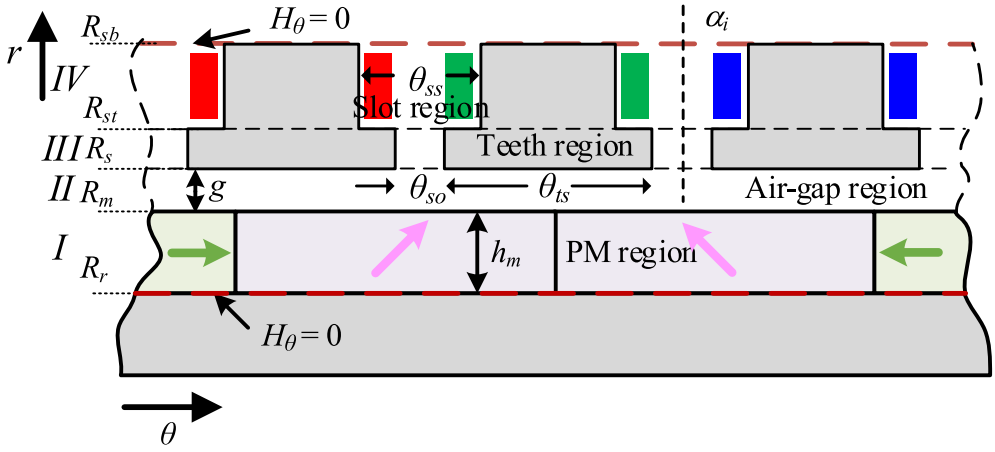

Fig. 1. 2-D analytical model.

of the rotor. The r-direction and θ-direction components of the magnetization vector M are solved in the Appendix.

$$\alpha_i = \frac{2\pi}{Q_s} i + \delta_{s0} \tag{1}$$

where α_i is the angular position of slot-opening.

3. Semi-analytical model of Halbach array permanent magnet machine

By introducing a magnetic vector potential, the magnetic field in each region can be computed by solving the following Laplace's or Poisson's equations:

$$\frac{\partial^2 A_z^k|_r}{\partial r^2} + \frac{1}{r}\frac{\partial A_z^k|_r}{\partial r} - \frac{K_\theta^2}{r^2} A_z^k|_r = \begin{cases} -\dfrac{\mu_0}{r}(M_\theta + jK_\theta M_r) & k = I \\ 0 & k = II \end{cases} \tag{2}$$

$$\frac{\partial^2 A_z^k|_r}{\partial r^2} + \frac{1}{r}\frac{\partial A_z^k|_r}{\partial r} - \left(\frac{V^k}{r}\right)^2 A_z^k|_r = \begin{cases} 0 & k = III \\ -\mu_{c,\theta}^k J_z & k = IV \end{cases} \tag{3}$$

where

$$K_\theta = diag[-N, \dots N] \tag{4}$$

$$V^k = \mu_{c,\theta}^k K_\theta [\mu_{c,r}^k]^{-1} K_\theta \quad k = III, IV. \tag{5}$$

The general solution for (2) and (3) are given as follows:

$$A_z^I = \left(\frac{r}{R_m}\right)^{\lambda_I} a_I + \left(\frac{R_r}{r}\right)^{\lambda_I} b_I + rG \tag{6}$$

$$A_z^{II} = \left(\frac{r}{R_s}\right)^{\lambda_{II}} a_{II} + \left(\frac{R_m}{r}\right)^{\lambda_{II}} b_{II} \tag{7}$$

$$A_z^{III} = W_{III}\left(\frac{r}{R_{st}}\right)^{\lambda_{III}} a_{III} + W_{III}\left(\frac{R_s}{r}\right)^{\lambda_{III}} b_{III} \tag{8}$$

$$A_z^{IV} = W_{IV}\left(\frac{r}{R_{sb}}\right)^{\lambda_{IV}} a_{IV} + W_{IV}\left(\frac{R_{st}}{r}\right)^{\lambda_{IV}} b_{IV} + r^2 F \tag{9}$$

where

$$G = \mu_0 (K_\theta^2 - I)^{-1} (M_\theta + j K_\theta M_r) \tag{10}$$

$$F = (V^{IV} - 4I)^{-1} \mu_{c,\theta}^{IV} J_z \tag{11}$$

where W_k and λ_k are the diagonal eigenvalue and the eigenvector matrix of V^k.

Based on the above general solutions, the interface continuity boundary conditions and Neumann boundary conditions are listed as follows:

$$A_z^I = A_z^{II}|_{r=R_m}, \quad H_\theta^I = H_\theta^{II}|_{r=R_m} \tag{12}$$

$$A_z^{II} = A_z^{III}|_{r=R_s}, \quad H_\theta^{II} = H_\theta^{III}|_{r=R_s} \tag{13}$$

$$A_z^{III} = A_z^{IV}|_{r=R_{st}}, \quad H_\theta^{III} = H_\theta^{IV}|_{r=R_{st}} \tag{14}$$

$$H_\theta^I = 0|_{r=R_r}, \quad H_\theta^{IV} = 0|_{r=R_{sb}}. \tag{15}$$

Then, the harmonic coefficients of each region can be computed by solving the following matrix equation.

$$MX = Y \tag{16}$$

with

$$M = \begin{bmatrix} M_{11} & M_{12} & 0 & 0 & 0 & 0 & 0 & 0 \\ M_{21} & M_{22} & M_{23} & M_{24} & 0 & 0 & 0 & 0 \\ M_{31} & M_{32} & M_{33} & M_{34} & 0 & 0 & 0 & 0 \\ 0 & 0 & M_{43} & M_{44} & M_{45} & M_{46} & 0 & 0 \\ 0 & 0 & M_{53} & M_{54} & M_{55} & M_{56} & 0 & 0 \\ 0 & 0 & 0 & 0 & M_{65} & M_{66} & M_{67} & M_{68} \\ 0 & 0 & 0 & 0 & M_{75} & M_{76} & M_{77} & M_{78} \\ 0 & 0 & 0 & 0 & 0 & 0 & M_{87} & M_{88} \end{bmatrix} \tag{17}$$

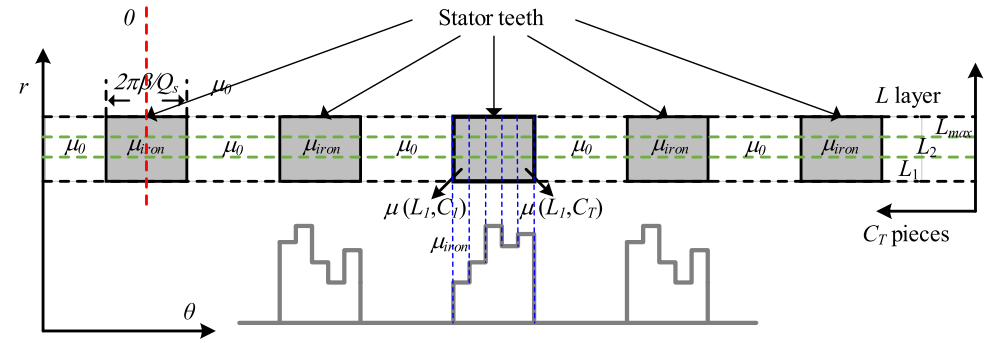

Fig. 2. Multilayer division of stator teeth.

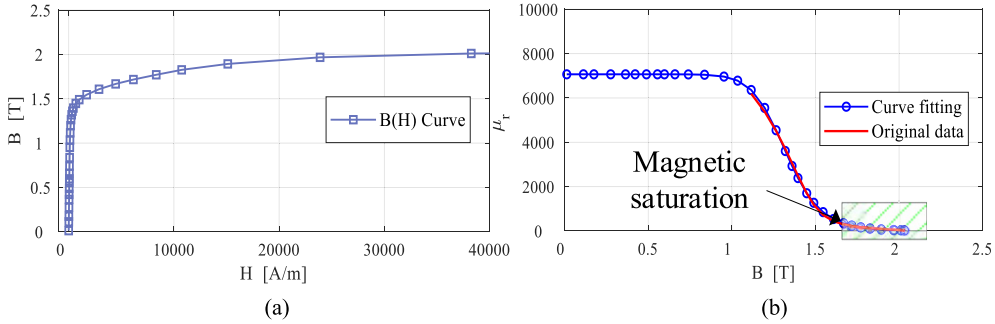

Fig. 3. Magnetic characteristic of WTG200. (a) B-H; (b) μ_r-B.

$$X = \begin{bmatrix} a_I & b_I & a_{II} & b_{II} & a_{III} & b_{III} & a_{IV} & b_{IV} \end{bmatrix}^T \tag{18}$$

$$Y = \begin{bmatrix} Y_1 & Y_2 & Y_3 & 0 & 0 & Y_6 & Y_7 & Y_8 \end{bmatrix}^T . \tag{19}$$

Moreover, the EPs of the Halbach array PMSM can be further predicted, as shown in the Appendix.

On the other hand, in order to more accurately consider magnetic saturation, each iron part can be divided into C_T individual regions along the θ-direction and L layer along the r-direction, as illustrated in Fig. 2. The Fourier coefficients of the l-th layer of the stator slots/teeth region are given in the Appendix.

For the PM machine, though the stator tooth is designed in the unsaturated region, the tooth tip behavior obvious saturation effect. The relative permeability of the saturation region can be calculated by the following equation [26]:

$$\mu_r(B) = \left(\frac{B_o}{H_o \mu_0}\right)\left(\frac{1}{1+(B/B_o)^{v-1}}\right) \tag{20}$$

where B_o, H_o, and v are the constants that depend on the core materials.

The silicon steel selected in this paper is WTG200, its B-H curve and B-μ_r curve are given in Fig. 3. The parameters B_o, H_o, and v are 1.32, 149.07, and 13.84 respectively.

The nonlinear iterative algorithm proposed in Fig. 4 is used to update the permeability of the saturated region.

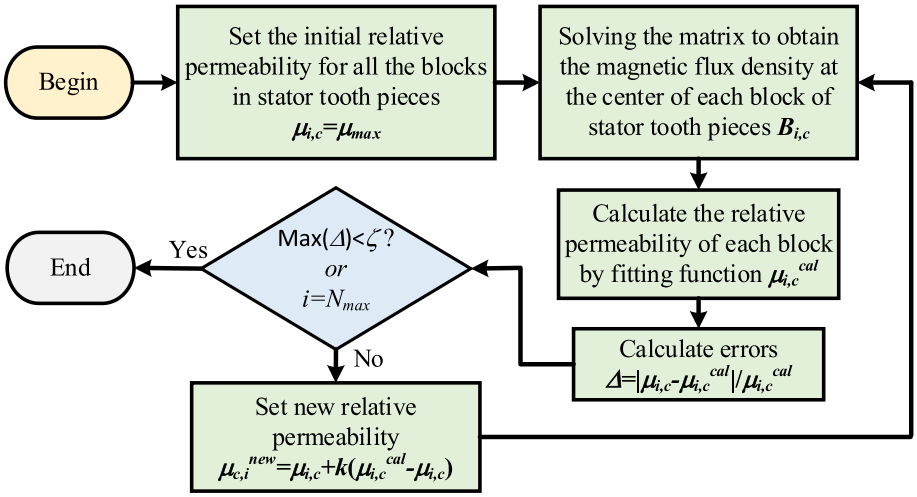

Fig. 4. Nonlinear iterative process considering potential local magnetic saturation.

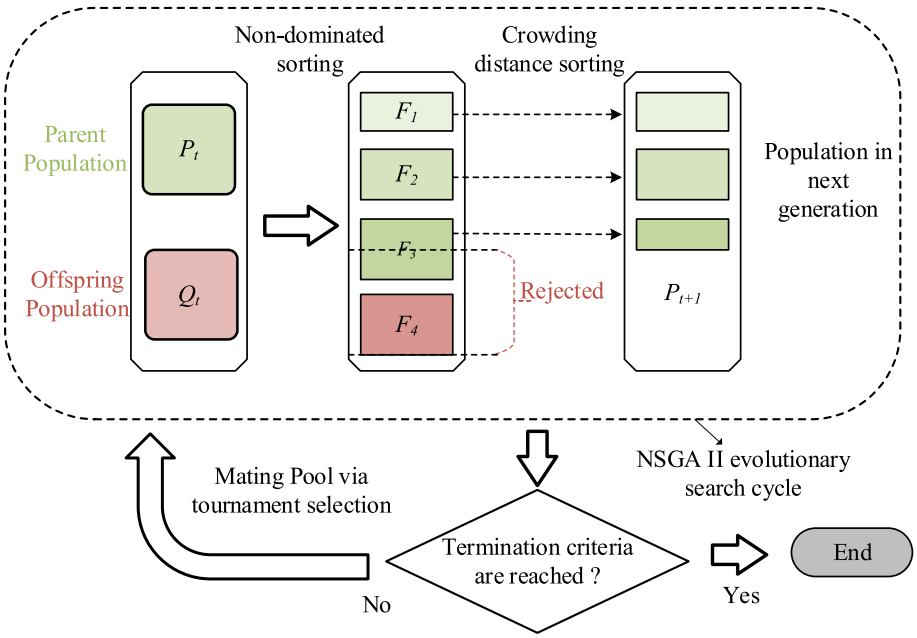

Fig. 5. The general structure of NSGA II.

4. Optimization process

The NSGA-II, which is a multi-objective optimization algorithm based on the Pareto optimal solution, was first proposed in 2002 [27]. In contrast to the traditional optimization algorithm, the NSGA-II adopts an elite strategy and crowding distances operator, which reduces the computation and achieves a fast and accurate performance search. The general structure of the NSGA-II algorithm is given in Fig. 5.

Table 2
Value range of design variables

Items	Symbol	Range
Slot opening angle	θ_{so}	1 ~ 5°
Air-gap length	g	0.5 ~ 4 mm
Thickness of PM	h_m	4 ~ 10 mm
Magnetization direction	φ_g	20 ~ 90°
Active stack length	L_{lef}	30 ~ 60 mm

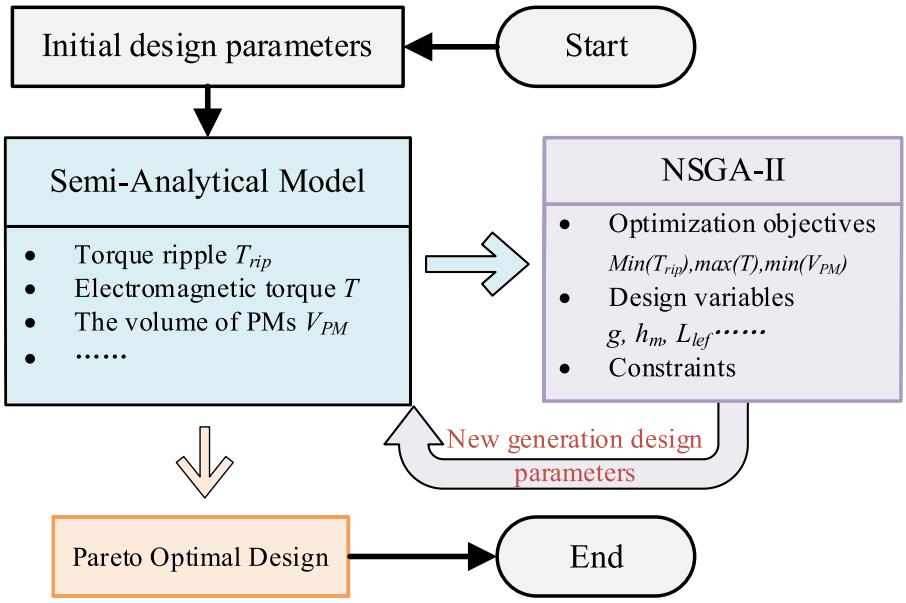

Fig. 6. Flow chart of the developed efficient multi-objective optimization strategy.

The optimization model that is proposed in this section mainly consists of objective functions and optimization parameters, etc. An essential parameter to evaluate the performance of the PMSM is the output torque T. The optimization process attempts to maximize output torque in a constrained volume. Torque ripple T_{rip}, on the other hand, is set as the optimization objective to ensure the high stability of the PM machine and reduce vibration and noise. Additionally, reducing the usage of rare-earth PM is one option to lower production costs. As a result, the volume consumption of rare-earth PM materials is set as the optimization objective, which is represented by V_{PM}.

The optimization objectives are listed below in accordance with the analysis mentioned above.

$$\text{Function}: [Max(T), Min(T_{rip}), Min(V_{PM})]. \tag{21}$$

In the optimization process, the parameters in Table 1 remain unchanged, then five independent design variables are selected, with the appropriate variation ranges shown in Table 2. The maximum number of generations is set at 120, with a specified limit of 20 for each generation. In the first stage, all variables

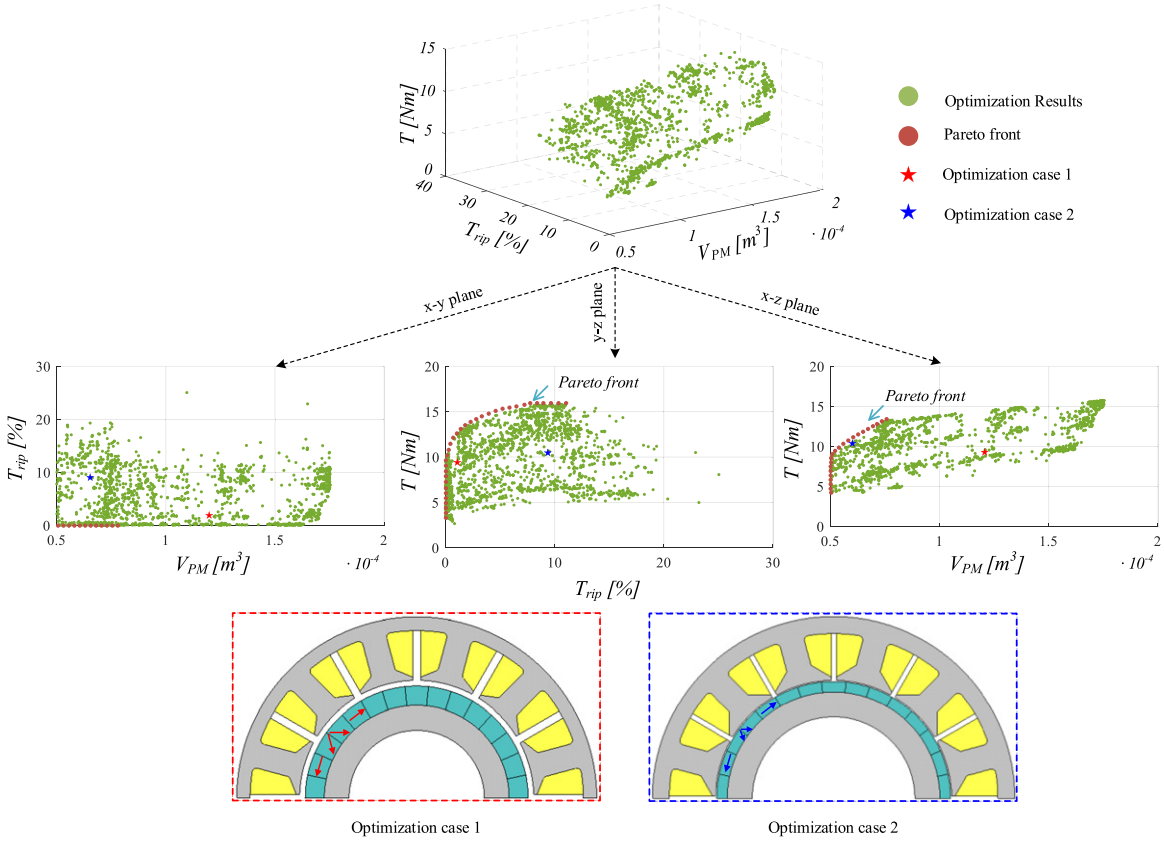

Fig. 7. Optimization results of the proposed method.

Table 3
Geometrical parameters of optimization cases

Items	Symbol	Case 1	Case 2
Radius of slot bottom	R_{sb}	74 mm	74 mm
Radius of slot top	R_{st}	53.5 mm	53.5 mm
Radius of stator bore	R_s	52 mm	52 mm
Outer radius of PM	R_m	49.5 mm	51.48 mm
Inner radius of PM	R_r	41 mm	46.83 mm
Slot width angle	θ_{ss}	20°	20°
Slot opening angle	θ_{so}	3.75°	2.22°
Air-gap length	g	2.5 mm	0.52 mm
Thickness of PM	h_m	8.5 mm	4.65
Magnet magnetization direction	φ_g	64°	73.3°
Active stack length	L_{lef}	50 mm	45.6 mm
Output torque	T	8.53 Nm	10.15 Nm
Torque Ripple	T_{rip}	1.72%	9.42%
Volume of PMs	V_{PM}	1.2e^{-4} m^3	6.5e^{-5} m^3

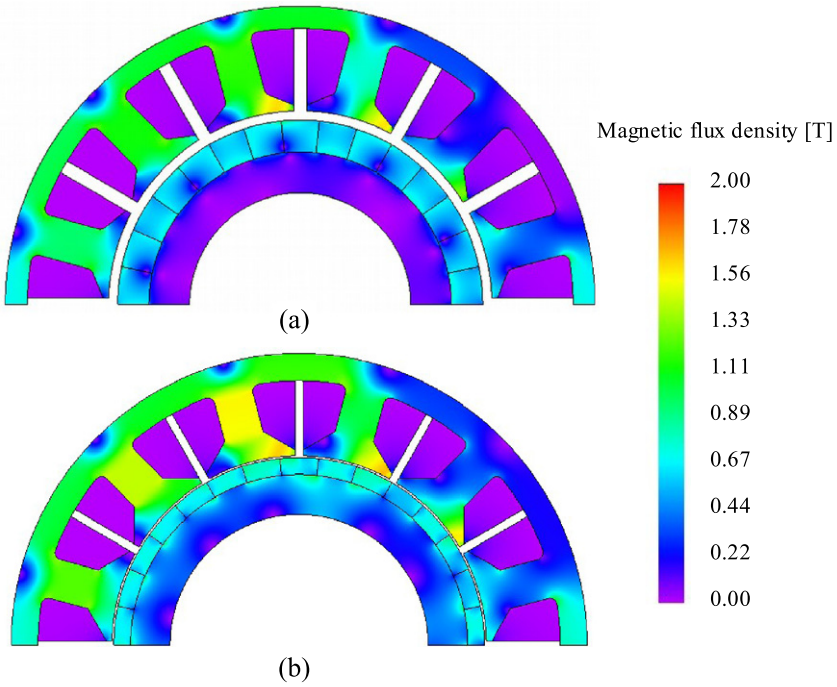

Fig. 8. FE models. (a) Optimization case 1; (b) Optimization case 2.

are randomly selected within the range of values to determine the initial population variable value. Then, the EPs can be obtained by nonlinear SAM. Figure 6 shows the flowchart of the developed efficient multi-objective optimization strategy.

The optimization results are presented in Fig. 7. On the *y*-*z* and *x*-*z* plane projections, two Pareto fronts can be identified clearly. To facilitate prototype manufacturing and satisfy the optimization objectives of maximum output torque ($Max\ (T)$), minimum torque ripple ($Min\ (T_{rip})$), and minimum PMs consumption ($Min\ (V_{PM})$), a case is selected from the *y*-*z* and *x*-*z* plane projections respectively, and satisfies the above two optimization objectives. The geometric parameters and objective function values of the two case parameters are given in Table 3.

5. Verification

In this section, according to the two optimization cases given in Table 3, their FE models are established to compare the EPs of the two cases, in terms of the cogging torque, back EMF, and electromagnetic torque. Furthermore, a Halbach prototype was manufactured based on the optimization results of Case 1, and the correctness of the developed optimization strategy was verified by experiments.

5.1. Finite-element model

The FE models of two optimization cases are established in the commercial FE software JMAG. Figure 8 shows the magnetic field of two optimization cases on load conditions.

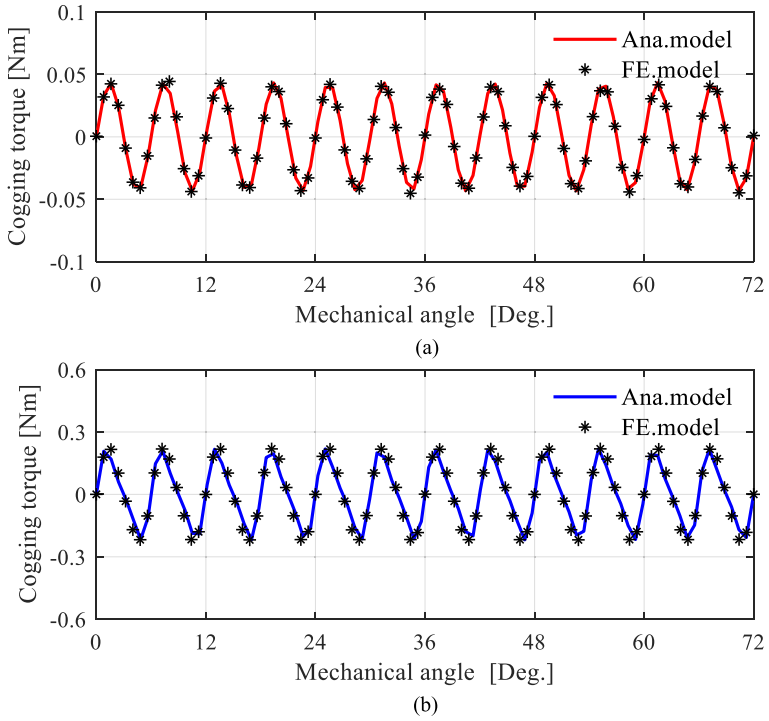

Fig. 9. Comparison of cogging torque. (a) Optimization case 1; (b) Optimization case 2.

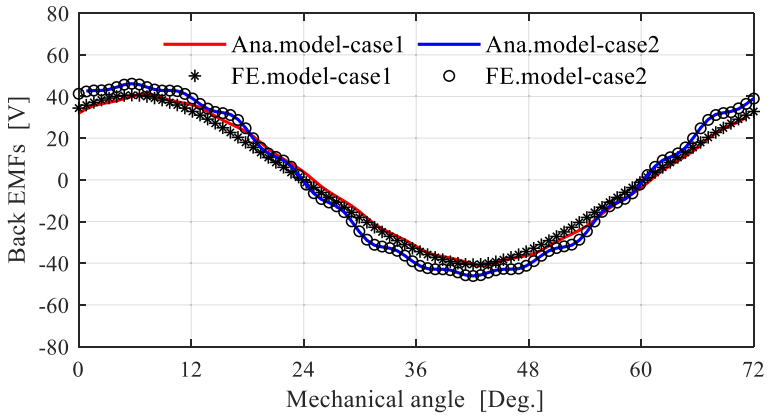

Fig. 10. Comparison of Back EMF. (a) Optimization case 1; (b) Optimization case 2.

Figure 9 shows the comparison of cogging torque. It is clear that the waveforms predicted by the nonlinear SAM are very consistent with the FE analysis results. In Fig. 10, the comparison of back EMF is given. The computation is carried out at 3000 r/min, and the amplitude of the phase back EMF of optimization cases 1 and 2 by SAM is 40.64 V and 45.72 V, respectively, while those by the FE model are 40.01 V and 45.31 V. The electromagnetic torque waveforms computed by using the proposed nonlinear

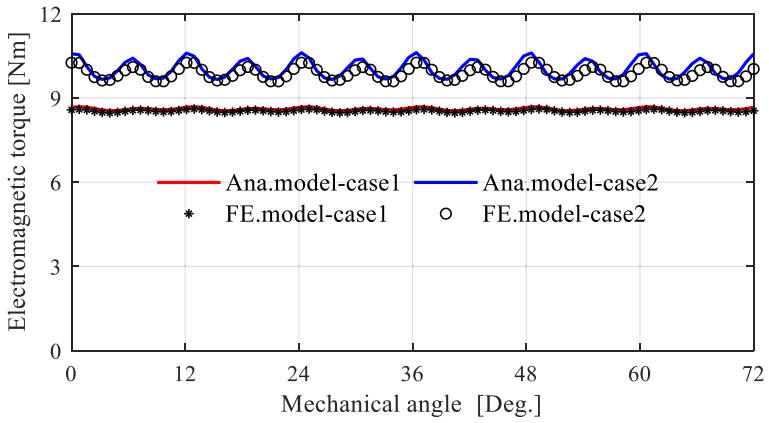

Fig. 11. Comparison of electromagnetic torque. (a) Optimization case 1; (b) Optimization case 2.

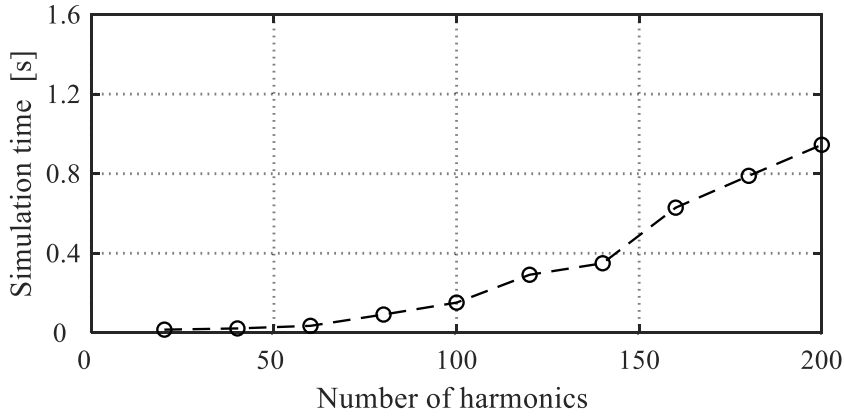

Fig. 12. Influence of the number of harmonics on computation time.

Table 4
Computation time comparisons of different calculation methods

	Linear SAM	Nonlinear SAM	Nonlinear FE model
Computation time	0.35 s	3.91 s	5.46 s

SAM and the FE model at rated current are shown in Fig. 11. It is clear that the waveforms from the two optimization cases and those from the FE analysis match very well.

Figure 12 shows the influence of the number of harmonics on the calculation time. To make a compromise between calculating efficiency and accuracy, the maximum harmonic order N for computation in this article is set to 140. Both analytical models and FE models are run on a PC with Intel (R) Core (TM) i7-7700k CPU @ 4.20GHz and 16 GB main memory under the WIN10 operating environment. The calculation time of different methods for single-step MFD is listed in Table 4. It can be seen that compared to the nonlinear FE model, nonlinear SAM is 28.4% faster. On the other hand, linear SAM has

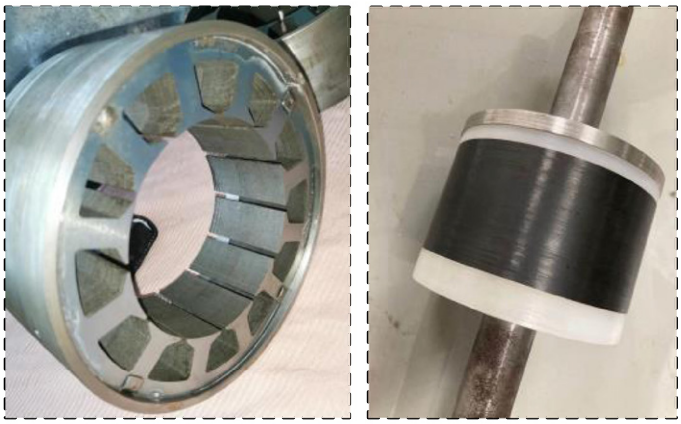

(a) (b)

Fig. 13. The stator and rotor of the prototype machine. (a) Stator; (b) Rotor.

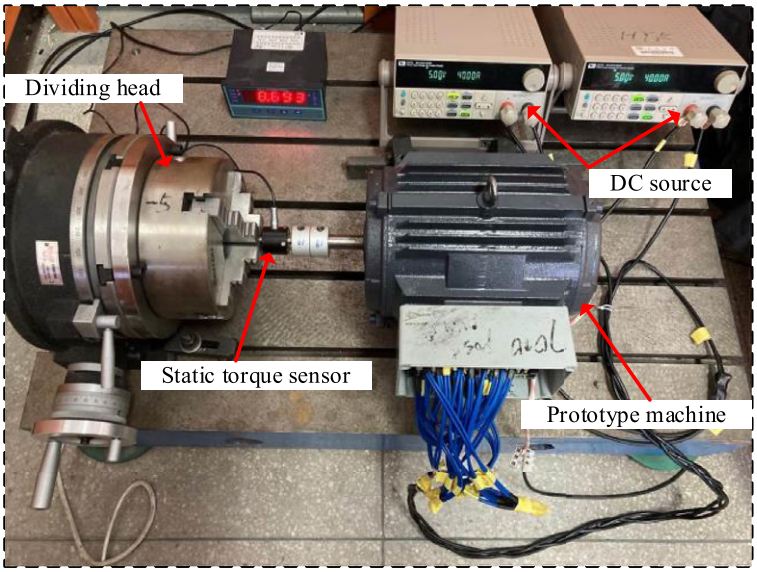

Fig. 14. Experimental setup for static torque measurement.

high computational efficiency and has important application prospects in the design and optimization of permanent magnet motors.

5.2. *Experimental validation*

To further verify the correctness and accuracy of the developed optimization strategy, a prototype is manufactured according to the design parameters of optimization case 1. The stator and rotor structure is shown in Fig. 13.

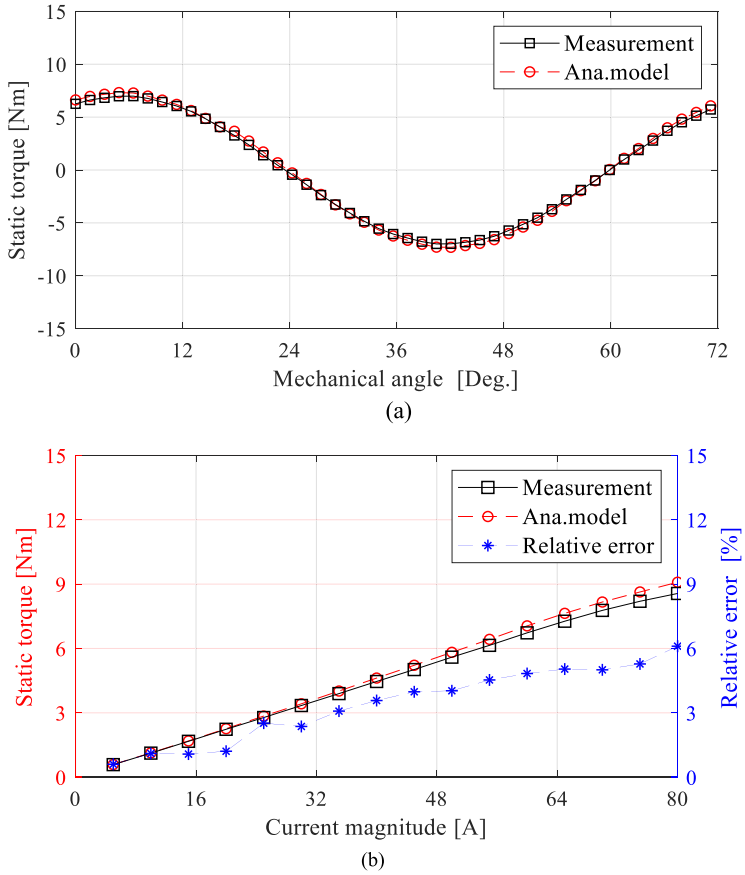

Fig. 15. Comparison of static torque. (a) The torque varies with the rotor position; (b) The maximum value of static torque varies with current.

To verify the torque-producing capacity of optimization case 1, static torque is measured. The experimental setup is shown in Fig. 14. As shown in Fig. 15, the waveform of static torque predicted by the proposed SAM agrees very well with the experimental result. As can be observed from Fig. 15(b), the relative error of the static torque predicted by the nonlinear SAM increases with a rise in current, but it is always at a reasonably low level. In particular, the static torque measurement result is 8.57 Nm when the phase current amplitude is 80 A (128% of rated current), whereas the calculated value is 9.09 Nm, and the relative error is only 6.07%.

The back EMF of the prototype was tested at 3800 r/min. The experimental devices are shown in Fig. 16. The comparison of phase-back EMF between the proposed nonlinear SAM and the experimental result is given in Fig. 17. The calculated amplitude of the phase-back EMF is 51.48 V, while the measured value is 49.6 V, and the relative error is only 3.8%, which meets the error requirement.

6. Conclusions

Although the Halbach array is known for about 50 years, its application to PM motors is an emerging field with great potential. To this end, this paper presents an efficient multi-objective optimization strategy

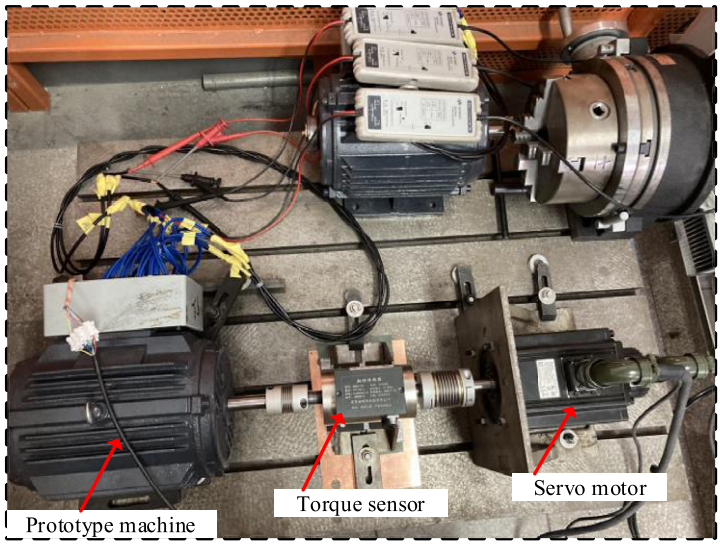

Fig. 16. Experimental setup for back EMF measurement.

for Halbach array PM synchronous machine, which combines HM technology and NSGA-II optimization algorithm. Then, a Halbach array PM machine is optimized by this optimization scheme, and two optimization cases are obtained. Additionally, a prototype is manufactured according to the optimization results, and the experimental results confirm the effectiveness of the developed optimization strategy. The optimization strategy developed in this paper has important theoretical significance and engineering reference value for other types of PM machines, especially for the axial flux PM machines equipped with a Halbach magnet array, which will significantly reduce the design and optimization time.

Acknowledgement

The authors gratefully acknowledge the support from the National Nature Science Foundation of China (Project Number: 52277036).

Appendix A: Magnetization source

The center position of the mth tangential magnetized PM is defined as

$$\begin{cases} \delta_m = \dfrac{2\pi}{p}(m-1) + \delta_0 \\ m = 1, 2, \ldots, p \end{cases} \tag{22}$$

where δ_0 is the initial angular position of the rotor.

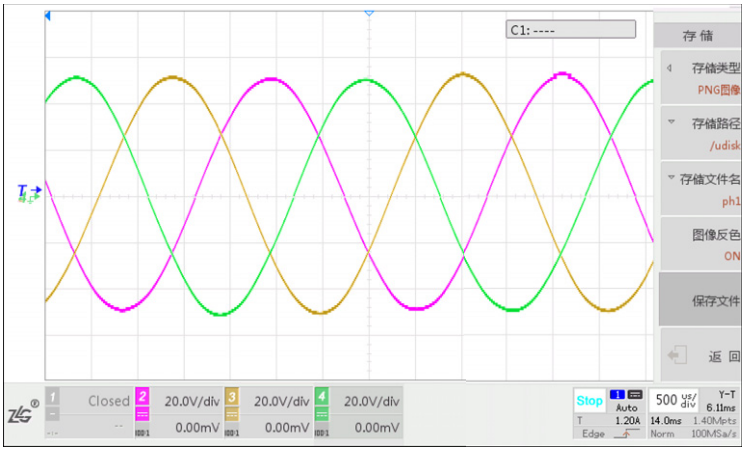

(a)

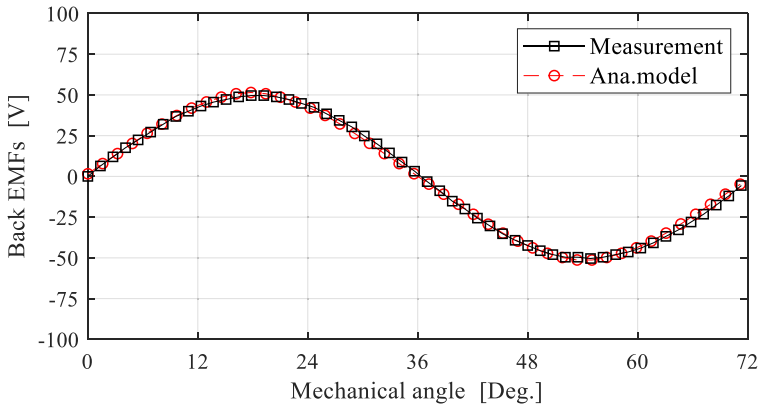

(b)

Fig. 17. Comparison of back EMFs. (a) Experimental results; (b) Comparison of analytical and experimental results.

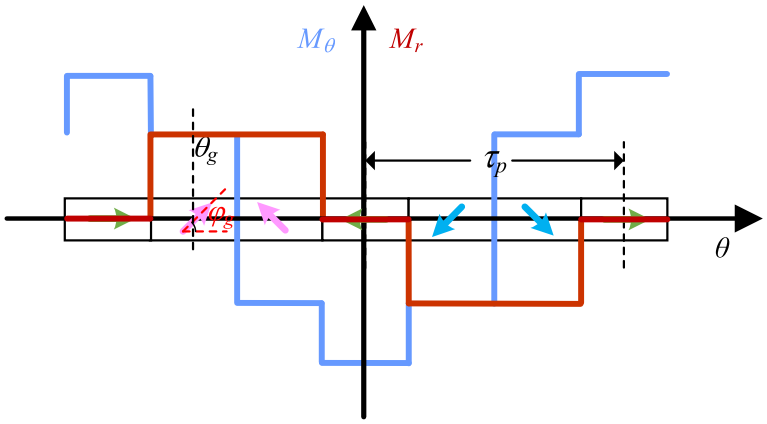

Fig. 18. Schematic of magnetization.

The center position θ_g of the gth PM is defined as:

$$\begin{cases} \theta_g = \dfrac{\pi(g-1)}{pt} \\ g = 1, 2, \ldots, 2t \end{cases} \tag{23}$$

where t represents the number of blocks per pole and here $t = 3$.

$$\hat{M}_{r,n} = \frac{1}{2\pi jn} \sum_{k=1}^{p} \sum_{g=1}^{2G} \frac{B_{rem}}{\mu_0} \cos(\varphi_g) \times \left\{ e^{jn\frac{(2g-1)\pi}{2pG}} - e^{jn\frac{(2g-3)\pi}{2pG}} \right\} e^{jn\delta_k}, \quad n \neq 0 \tag{24}$$

$$\hat{M}_{\theta,n} = \frac{1}{2\pi jn} \sum_{k=1}^{p} \sum_{g=1}^{2G} \frac{B_{rem}}{\mu_0} \sin(\varphi_g) \times \left\{ e^{jn\frac{(2g-1)\pi}{2pG}} - e^{jn\frac{(2g-3)\pi}{2pG}} \right\} e^{jn\delta_k}, \quad n \neq 0 \tag{25}$$

Schematic of magnetization is shown in Fig. 18.

Appendix B: Electromagnetic performance

The electromagnetic torque T_{em} (in on-load condition) and cogging torque T_c (in no-load condition) can be obtained [13].

$$T = \frac{L_{lef} R_g^2}{\mu_0} \int_0^{2\pi} B_r^{II}(R_g, \theta) B_\theta^{II}(R_g, \theta) d\theta. \tag{26}$$

The flux linkage of i-th stator slot coil could be computed by

$$\varphi_{1,i} = L_{lef} \frac{N_c}{S} \int_{\alpha_i - \frac{\theta_{ss}}{2}}^{\alpha_i - \frac{\theta_{ss}}{2} + d} \int_{R_{st}}^{R_{sb}} A_z^{IV}(r, \theta) dr d\theta \tag{27}$$

$$\varphi_{2,i} = L_{lef} \frac{N_c}{S} \int_{\alpha_i + \frac{\theta_{ss}}{2} - d}^{\alpha_i + \frac{\theta_{ss}}{2}} \int_{R_{st}}^{R_{sb}} A_z^{IV}(r, \theta) dr d\theta. \tag{28}$$

The total flux linkage can be obtained.

$$\begin{bmatrix} \Psi_a \\ \Psi_b \\ \Psi_c \end{bmatrix} = \begin{bmatrix} \Psi_{1,a} \\ \Psi_{1,b} \\ \Psi_{1,c} \end{bmatrix} + \begin{bmatrix} \Psi_{2,a} \\ \Psi_{2,b} \\ \Psi_{2,c} \end{bmatrix} \tag{29}$$

where

$$\begin{bmatrix} \Psi_{1,a} \\ \Psi_{1,b} \\ \Psi_{1,c} \end{bmatrix} = C_1 \begin{bmatrix} \varphi_{1,1} & \varphi_{1,2} & \cdots & \varphi_{1,Q_s} \end{bmatrix}^T \tag{30}$$

$$\begin{bmatrix}\Psi_{2,a}\\ \Psi_{2,b}\\ \Psi_{2,c}\end{bmatrix} = C_2\begin{bmatrix}\varphi_{2,1} & \varphi_{2,2} & \cdots & \varphi_{2,Q_s}\end{bmatrix}^T. \tag{31}$$

Then, the back EMFs can be calculated.

$$\begin{bmatrix}E_a\\ E_b\\ E_c\end{bmatrix} = -\frac{d}{dt}\begin{bmatrix}\Psi_a\\ \Psi_b\\ \psi_c\end{bmatrix}. \tag{32}$$

Appendix C: Fourier coefficients of *l*-th layer

The Fourier coefficients of the l-th layer of the stator slots/teeth region can be obtained by

$$\hat{\mu}_n^l = \begin{cases} (1-\beta)\mu_0 + \dfrac{\beta}{Q_s C_T}\displaystyle\sum_{i=1}^{Q_s}\sum_{c=1}^{C_T}\mu_{i,c} & n=0 \\ \displaystyle\sum_{i=1}^{Q_s}\frac{\mu_0}{2\pi jn}e^{jn\pi\frac{2(i-1)-\beta}{Q_s}}\left[1-e^{jn\pi\frac{2(\beta-1)}{Q_s}}\right] & \\ \quad+\displaystyle\sum_{i=1}^{Q_s}\sum_{c=1}^{C_T}\frac{\mu_{i,c}}{2\pi jn}e^{\frac{\beta C_T-2(i-1)C_T-2\beta c}{Q_s C_T}}\left[e^{jn\pi\frac{2\beta}{Q_s C_T}}-1\right] & n\neq 0 \end{cases} \tag{33}$$

where $\mu_{i,\,c}$ is the permeability in c-th piece of the i-th iron part.

References

[1] M.U. Lampérth, A.C. Malloy, A. Mlot and M. Cordner, Assessment of axial flux motor technology for hybrid powertrain integration, *World Electric Vehicle Journal* **7**(2) (2015), 2, doi:10.3390/wevj7020187.

[2] Z. Yang, F. Shang, I.P. Brown and M. Krishnamurthy, Comparative study of interior permanent magnet, induction, and switched reluctance motor drives for EV and HEV applications, *IEEE Transactions on Transportation Electrification* **1**(3) (2015), 245–254, doi:10.1109/TTE.2015.2470092.

[3] L. Xu, X. Zhu, W. Fan, C. Zhang, L. Zhang and L. Quan, Comparative analysis and design of partitioned stator hybrid excitation axial flux switching PM motors for in-wheel traction applications, *IEEE Transactions on Energy Conversion* **37**(2) (2022), 1416–1427, doi:10.1109/TEC.2021.3130475.

[4] L. Xu, H. Liu, X. Zhu, W. Fan, C. Zhang, L. Zhang et al., Multiple-mode current control for a hybrid-excitation axial flux switching permanent magnet motor considering driving cycles, *IEEE Transactions on Industrial Electronics* **71**(1) (2024), 204–214, doi:10.1109/TIE.2023.3243278.

[5] Z. Zhu, Y. Huang, J. Dong, F. Peng and Y. Yao, Rotor eddy current loss reduction with permeable retaining sleeve for permanent magnet synchronous machine, *IEEE Transactions on Energy Conversion* **35**(2) (2020), 1088–1097. doi:10.1109/TEC.2020.2966674.

[6] H.S. Zhang, Z.X. Deng, M.L. Yang, Y. Zhang, J.Y. Tuo and J. Xu, Analytical prediction of Halbach array permanent magnet machines considering finite tooth permeability, *IEEE Transactions on Magnetics* **56**(6) (2020), 1–10. doi:10.1109/TMAG.2020.2982844.

[7] H. Zhao, C. Liu, Z. Song and J. Yu, A fast optimization scheme of coaxial magnetic gears based on exact analytical model considering magnetic saturation, *IEEE Transactions on Industry Applications* **57**(1) (2021), 437–447. doi:10.1109/TIA.2020.3040142.

[8] B. Guo, Y. Huang, F. Peng and J. Dong, A new hybrid method for magnetic field calculation in IPMSM accounting for any rotor configuration, *IEEE Transactions on Industrial Electronics* **66**(7) (2019), 5015–5024. doi:10.1109/TIE.2018.2868252.

[9] T. Lubin, S. Mezani and A. Rezzoug, Exact analytical method for magnetic field computation in the air gap of cylindrical electrical machines considering slotting effects, *IEEE Transactions on Magnetics* **46**(4) (2010), 1092–1099, doi:10.1109/TMAG.2009.2036257.

[10] R.L.J. Sprangers, J.J.H. Paulides, B.L.J. Gysen, J. Waarma and E.A. Lomonova, Semianalytical framework for synchronous reluctance motor analysis including finite soft-magnetic material permeability, *IEEE Transactions on Magnetics* **51**(11) (2015), 1–4, doi:10.1109/TMAG.2015.2442419.

[11] R.L.J. Sprangers, J.J.H. Paulides, B.L.J. Gysen and E.A. Lomonova, Magnetic saturation in semi-analytical harmonic modeling for electric machine analysis, *IEEE Transactions on Magnetics* **52**(2) (2016), 1–10. doi:10.1109/TMAG.2015.2480708.

[12] Z. Djelloul-Khedda, K. Boughrara, F. Dubas and R. Ibtiouen, Nonlinear analytical prediction of magnetic field and electromagnetic performances in switched reluctance machines, *IEEE Transactions on Magnetics* **53**(7) (2017), 1–11, doi:10.1109/TMAG.2017.2679686.

[13] Z. Djelloul-Khedda, K. Boughrara, R. Ibtiouen and F. Dubas, NonLinear analytical calculation of magnetic field and torque of switched reluctance machines, in: *2016 International Conference on Electrical Sciences and Technologies in Maghreb (CISTEM)*, IEEE, 2016, pp. 1–8. doi:10.1109/CISTEM.2016.8066773.

[14] Z. Djelloul-Khedda, K. Boughrara, F. Dubas, A. Kechroud and A. Tikellaline, Analytical prediction of iron-core losses in flux-modulated permanent-magnet synchronous machines, *IEEE Transactions on Magnetics* **55**(1) (2019), 1–12, doi:10.1109/TMAG.2018.2877164.

[15] H. Zhao, K.T. Chau, T. Yang, Z. Song and C. Liu, A novel quasi-3D analytical model for axial flux motors considering magnetic saturation, *IEEE Transactions on Energy Conversion* **37**(2) (2022), 1358–1368, doi:10.1109/TEC.2021.3132618.

[16] B. Guo et al., Nonlinear semianalytical model for axial flux permanent-magnet machine, *IEEE Transactions on Industrial Electronics* **69**(10) (2022), 9804–9816, doi:10.1109/TIE.2022.3159952.

[17] D.-K. Lim, D.-K. Woo, H.-K. Yeo, S.-Y. Jung, J.-S. Ro and H.-K. Jung, A novel surrogate-assisted multi-objective optimization algorithm for an electromagnetic machine design, *IEEE Transactions on Magnetics* **51**(3) (2015), 1–4, doi:10.1109/TMAG.2014.2359452.

[18] H. Chen, W. Yan, J.J. Gu and M. Sun, Multiobjective optimization design of a switched reluctance motor for low-speed electric vehicles with a Taguchi–CSO algorithm, *IEEE/ASME Transactions on Mechatronics* **23**(4) (2018), 1762–1774, doi:10.1109/TMECH.2018.2839619.

[19] M. Ruba et al., Synchronous reluctance machine geometry optimisation through a genetic algorithm based technique, *IET Electric Power Applications* **12**(3) (2018), 431–438, doi:10.1049/iet-epa.2017.0455.

[20] J.H. Lee, J.-W. Kim, J.-Y. Song, Y.-J. Kim and S.-Y. Jung, A novel memetic algorithm using modified particle swarm optimization and mesh adaptive direct search for PMSM design, *IEEE Transactions on Magnetics* **52**(3) (2016), 1–4, doi:10.1109/TMAG.2015.2482975.

[21] Y. Ma, T.W. Ching, W.N. Fu and S. Niu, Multi-objective optimization of a direct-drive dual-structure permanent magnet machine, *IEEE Transactions on Magnetics* **55**(10) (2019), 1–4, doi:10.1109/TMAG.2019.2922475.

[22] Y. Duan, R.G. Harley and T.G. Habetler, A useful multi-objective optimization design method for PM motors considering nonlinear material properties, in: *2009 IEEE Energy Conversion Congress and Exposition*, IEEE, 2009, pp. 187–193. doi:10.1109/ECCE.2009.5316144.

[23] X. Liu, C. Hu, X. Li, J. Gao and S. Huang, An online data-driven multi-objective optimization of a permanent magnet linear synchronous motor, *IEEE Transactions on Magnetics* **57**(7) (2021), 1–4, doi:10.1109/TMAG.2021.3059513.

[24] B. Ma, G. Lei, J. Zhu, Y. Guo and C. Liu, Application-oriented robust design optimization method for batch production of permanent-magnet motors, *IEEE Transactions on Industrial Electronics* **65**(2) (2018), 1728–1739, doi:10.1109/TIE.2017.2748046.

[25] X. Zhu, W. Wu, L. Quan, Z. Xiang and W. Gu, Design and multi-objective stratified optimization of a less-rare-earth hybrid permanent magnets motor with high torque density and low cost, *IEEE Transactions on Energy Conversion* **34**(3) (2019), 1178–1189, doi:10.1109/TEC.2018.2886316.

[26] A. Hemeida and P. Sergeant, Analytical modeling of surface PMSM using a combined solution of Maxwell–s equations and magnetic equivalent circuit, *IEEE Transactions on Magnetics* **50**(12) (2014), 1–13, doi:10.1109/TMAG.2014.2330801.

[27] K. Deb, A. Pratap, S. Agarwal and T. Meyarivan, A fast and elitist multiobjective genetic algorithm: NSGA-II, *IEEE Transactions on Evolutionary Computation* **6**(2) (2002), 182–197, doi:10.1109/4235.996017.